Modification of Amiet's model for turbulence-ingestion noise prediction in rotors

Piccolo, Andrea; Zamponi, Riccardo; Avallone, Francesco; Ragni, Daniele

DOI
10.1121/10.0037185

Publication date
2025

Document Version
Final published version

Published in
Journal of the Acoustical Society of America

JULY 16 2025

Modification of Amiet's model for turbulence-ingestion noise prediction in rotors[a)]

Andrea Piccolo ; Riccardo Zamponi ; Francesco Avallone ; Daniele Ragni

J. Acoust. Soc. Am. 158, 461–475 (2025)
https://doi.org/10.1121/10.0037185

JASA ARTICLE

Modification of Amiet's model for turbulence-ingestion noise prediction in rotors[a)]

Andrea Piccolo,[1,b)] Riccardo Zamponi,[1,2] Francesco Avallone,[3] and Daniele Ragni[1]

[1]*Department of Flow Physics and Technology, Technische Universiteit Delft, Kluyverweg 1 2629HS, Delft, Netherlands*

[2]*Environmental and Applied Fluid Dynamics Department, von Karman Institute for Fluid Dynamics, Waterloosesteenweg 72 B-1640, Sint-Genesius-Rode, Belgium*

[3]*Dipartimento di Ingegneria Meccanica e Aerospaziale (DIMEAS), Politecnico di Torino, Corso Duca degli Abruzzi 24 10129, Torino, Italy*

ABSTRACT:

Amiet's model for turbulence-ingestion noise prediction for rotors is adapted to incorporate pointwise velocity measurements as input. This is accomplished by using an inverse strip theory approach and transforming the three-dimensional turbulence spectrum, which models inflow conditions, into a one-dimensional term. This latter modification enhances the low-fidelity prediction tool in two key ways. First, it enables its application in cases where turbulence modeling is unavailable, or detailed inflow characterization is impractical. In this way, for example, hot-wire anemometry measurements of the incoming turbulence can be used to compute the acoustic prediction. Second, since the conversion of the turbulence term entails introducing two new functions describing spanwise and axial turbulence correlations; this approach establishes a framework for Amiet's theory in which the contributions to turbulence alteration and noise scattering are separated and represented individually. This "modular" structure enables independent analysis and modeling of these contributions, facilitating the application of Amiet's model to complex flow configurations and rotor geometries. The proposed methodology is successfully validated through experimental measurements of a simplified axial-flight turbulence-interaction setup, where a two-bladed propeller interacts with grid-generated turbulence at three different advance ratios.

 https://doi.org/10.1121/10.0037185

(Received 4 April 2025; revised 18 June 2025; accepted 26 June 2025; published online 16 July 2025)

[Editor: Eric Greenwood] Pages: 461–475

I. INTRODUCTION

The field of urban air mobility (UAM) has experienced rapid expansion in recent years, with a diverse range of potential applications envisioned for this technology. This has driven considerable growth in research efforts. In particular, significant focus is being directed toward the optimization of the acoustic performance of rotors, dominated by aerodynamic noise, as it represents one of the main obstacles to the diffusion of UAM (Rizzi *et al.*, 2020; Boucher *et al.*, 2024). Among the various flow-induced noise sources, turbulence-ingestion noise (TIN), generated by the interaction of incoming turbulence with the rotor, is a key area of attention (Thurman *et al.*, 2025).

This attention is first due to the highly turbulent flows characterizing urban environments, where UAM vehicles are planned to operate and where the minimization of acoustic emissions is crucial. Second, the importance of TIN research is growing as, for UAM vehicles, the broadband noise component not only prevails over the tonal one—which represents a key difference from previously studied rotorcraft applications—but also practically overlaps with the human hearing range (Zawodny *et al.*, 2016; Greenwood *et al.*, 2022; Thurman *et al.*, 2025). Last, the ongoing and extensive investigation into this area is driven by the complexity and diversity of the physical mechanisms involved (Piccolo *et al.*, 2024; Zamponi *et al.*, 2021). These deserve particular attention, as the accuracy of their description and modeling affects the reliability of low-fidelity noise prediction, which represents the most suitable tool for the optimization phase because of the lower computational cost compared to numerical simulations.

TIN, investigated and modeled for the first time by Sharland (1964), is produced by the unsteady surface pressure induced by turbulence interacting with the blades. A wide range of turbulence scales, ranging from the diameter of the rotor to the thickness of the blade, contributes to the sound generation (Simonich *et al.*, 1986). These turbulent structures are deformed by the rotor-induced streamtube, as first shown by Hanson (1974). This implies that, even assuming a state of homogeneity and isotropy for the turbulence far away from the rotor, noise is actually generated by the interaction of anisotropic turbulence with the blades. In particular, Hanson (1974) showed that the contracting

[a)]This paper is part of a special issue on "Advanced Air Mobility Noise: Predictions, Measurements, and Perception."

[b)]Email: a.piccolo@tudelft.nl

streamtube induces a stretching of the turbulent structures into elongated eddies, which are hence prone to be cut multiple times by the passage of different blades. This mechanism, defined as blade-to-blade correlation, causes partially coherent unsteady surface pressure on different blades, adding quasi-tonal peaks at the blade-passage frequency (BPF) harmonics to the mainly broadband characteristics of the TIN spectra. This narrowband noise feature is also referred to as haystacking (Raposo and Azarpeyvand, 2024). Hanson (1974) also developed a model for sound prediction, using flow-field measurements and surface pressure as input to characterize the statistical distribution of eddies. These were incorporated into random pulse-modulation theory to calculate the unsteady blade forces and the resulting noise.

Hanson's work laid the foundation for the study of Majumdar and Peake (1998), who employed rapid distortion theory (RDT), following Goldstein's formulation (Goldstein, 1978), to account for turbulence distortion in the streamtube in the case of an aero engine. The same approach was also used by Simonich *et al.* (1986, 1990) and Amiet *et al.* (1990) to investigate TIN in helicopters. Their findings demonstrated that turbulence distortion is influenced by the operating conditions of the rotor, since the contraction of the streamtube varies with the operating regime. Specifically, they observed significant turbulence alteration at low free-stream velocities, such as in hover and low-speed ascent, where the streamtube contraction is most pronounced. In contrast, in forward flight and high-speed ascent, the deformation of turbulent structures is less pronounced. The model was also capable of accounting for the effects of blade-to-blade correlation (referred to as "B2B" from now on).

The theory of Amiet (1976) was based on the formulation developed for a wing in rectilinear motion, for which the radiated sound was related to the inflow-turbulence spectrum through the aerodynamic and acoustic response of a linearized airfoil, i.e., a flat plate (Amiet, 1975). This framework was extended to the rotational motion by assuming that it could be approximated to a rectilinear one. This assumption holds for acoustic frequencies significantly larger than the rotor rotational speed. Amiet's approach overcame the low-frequency limitations of the earlier model by Homicz and George (1974), who treated the blade as a moving dipole source by relying on a low-frequency response function and a blade-compactness assumption to compute unsteady loading and the resulting acoustic pressure field. Amiet's model has thus emerged as the most robust and feasible theory for low-fidelity TIN prediction. This has recently been confirmed by Raposo and Azarpeyvand (2024), which proved that the model can effectively capture both broadband characteristics and narrowband haystacking features. despite all the assumptions regarding blade geometry and inflow conditions.

Therefore, in a simple turbulence-rotor interaction configuration, two intrinsically related and consecutive physical mechanisms characterize the interaction: the elongation of turbulent structures due to streamtube contraction and their subsequent repeated chopping by multiple blades. In theory, another physical mechanism is expected to influence turbulence alteration during its interaction with the blades, thereby affecting noise generation and prediction. This is the deformation induced by the flow that accelerates along the leading edge itself, investigated and modeled by several studies (Santana *et al.*, 2016; dos Santos *et al.*, 2022; Piccolo *et al.*, 2024), which proved its relevance in high-frequency noise in the 2D regime in the case of blunt airfoils. No studies currently investigate or model this effect for rotating blades, but this is expected to play a significant role in the case of small-scale turbulence relative to the leading-edge radius, e.g., for thick blades, and at significant pitch angles (Piccolo *et al.*, 2024). A conceptual representation of turbulence alteration in the interaction with a rotor is reported in Fig. 1.

The studies mentioned above clearly demonstrate the complexity of the physical mechanisms underlying TIN generation and modeling. Moreover, the growing variety of configurations and operating conditions envisioned for UAM vehicles has led to increasingly heterogeneous and complex geometries and inflow conditions. In addition to the previously discussed mechanisms, these factors introduce new and unexplored interactions that can influence noise generation.

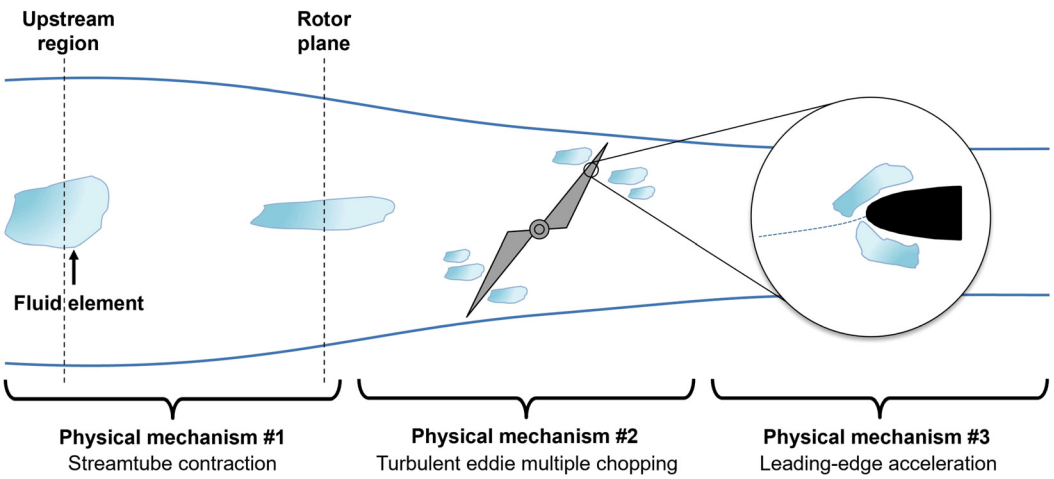

FIG. 1. Physical mechanisms undergone by turbulence approaching a rotor.

https://doi.org/10.1121/10.0037185

This highlights the need for further research on low-fidelity noise prediction, emphasizing the importance of direct physical investigations before engaging in any modeling efforts (Goldschmidt *et al.*, 2022). This study goes in this direction by proposing a modification to Amiet's model that allows pointwise flow measurements with local velocity information to be used as input. Indeed, the canonical formulation of Amiet's model relies on a 3D turbulence input, which is notably difficult to measure and compute, both experimentally and numerically. Calculating such a spectrum requires knowledge of turbulent velocity fluctuations throughout an entire volume of the flow field, within which the 3D two-point correlation must first be computed and then integrated. The final accuracy of the result is then directly influenced by both the extent of the volume and the spatial resolution. Glegg *et al.* (2013; Glegg *et al.*, 2015) introduced a time-domain approach—not based on Amiet's theory—to pursue the same goal, but the model still requires measuring the four-dimensional velocity correlation function in the rotor plane, which is not always feasible. Similar limitations affect the prediction method developed by Brooks and Burley (2004) for blade-wake interaction (BWI) noise, which is based on the measured leading-edge surface pressures as input. By retaining Amiet's frequency-based framework and reducing the 3D turbulence input to a 1D, this study enables the use of hot-wire measurements as input in experimental configurations or pointwise acquisitions in numerical simulations. This formulation makes the model a simple yet effective hybrid tool for estimating acoustic performance and assessing inflow effects in complex configurations where sophisticated measurements are impractical and inflow modeling is unavailable. Additionally, it enables the application of turbulence-distortion models developed for rectilinear motion to rotors, potentially improving predictions in configurations where the distortion due to leading-edge bluntness is significant. The proposed methodology is validated with the results of an experimental campaign carried out to investigate the noise generated by a two-bladed propeller operating at low Reynolds at three different advance ratios. This also enables a systematic assessment of Amiet's model accuracy across various operating conditions, addressing a gap in the existing literature.

The paper is structured as follows: Sec. II reports the information about the experimental setup and a quick overview of Amiet's model for TIN in rotors. The proposed methodological modifications and their validation are presented in Sec. III. Conclusions are drawn in Sec. IV.

II. METHODOLOGY

A. Experimental setup

The experimental campaign has been conducted in the anechoic wind tunnel (A-Tunnel) of the Flow Physics and Technology Department of TU Delft. This facility consists of a vertical open-jet wind tunnel, with the test section being an anechoic chamber lined with melamine wedges. To avoid potential acoustic reflections, the metal grids that typically cover the sound-absorbing foam on the floor were removed during the noise measurements. A detailed description and characterization of this wind tunnel is provided by Merino-Martínez *et al.* (2020). A picture of the rig in the anechoic

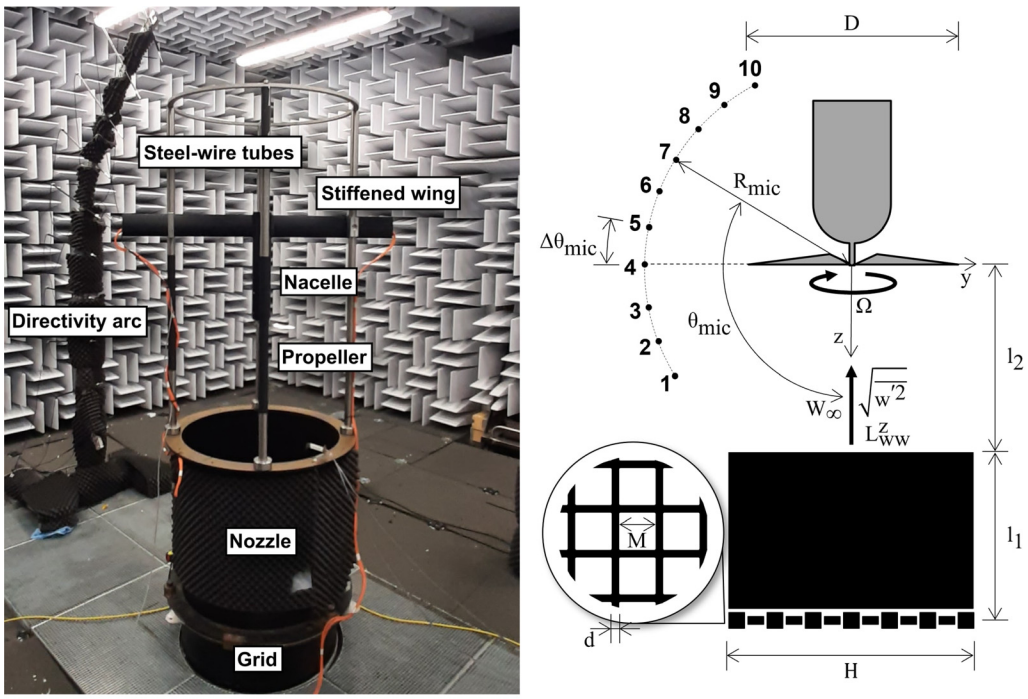

(A) (B)

FIG. 2. (A) Picture of the experimental setup mounted in the A-Tunnel at TU Delft, (B) descriptive sketch of the setup with the main dimensions, distances, and operational parameters.

chamber is reported in Fig. 2, which also shows a qualitative sketch of the experimental setup with the main dimensions, distances, and operational parameters. The reference system is consistent with the notation used in Amiet's formulation (Amiet, 1989). The axial direction, aligned with the free-stream velocity but oriented in the opposite direction, is denoted by z, with the corresponding velocity component being w. The origin is set at the rotor hub and the x and y axes—whose respective velocity components are u and v—lie in the rotor plane, forming a right-hand coordinate system.

A constant-section circular nozzle with diameter H and length l_1 equal to 0.60 m has been placed at the exit of the tunnel. Turbulence is generated by a rectangular grid positioned upstream of the constant-section nozzle to minimize background noise. The grid consists of rectangular bars with a width of $d = 0.01$ m and a mesh length of $M = 0.10$ m, as shown in the detail of Fig. 2. The free-stream velocity at the nozzle exit is $W_\infty = 9.5\,\mathrm{ms}^{-1}$. Turbulence is characterized by the turbulence intensity, which quantifies the strength of velocity fluctuations relative to the mean flow, and the integral length scale, which estimates the size of the energy-containing eddies. The turbulence intensity is $\sqrt{\overline{w'^2}}/W_\infty = 6$ %, where w' denotes fluctuations of the axial velocity component, and the integral length scale is $L^z_{ww} = 0.018$ m. These flow characteristics have been obtained through hot-wire measurements, as described in Sec. II A 2, conducted at the nozzle exit without the propeller.

The propeller and test rig used in this experimental campaign are the same as used by Grande *et al.* (2022b). The test rig consists of an aluminum nacelle with a diameter of 0.05 m, which stems from a stiffened hollow aluminum NACA-0012 wing [Standard Airfoil Profile, National Advisory Committee for Aeronautics (NACA), Washington, DC] with a 0.06 m chord. The entire structure is suspended above the tunnel nozzle by four steel-wire tubes, each with a diameter of 2 cm, secured to the tunnel to minimize vibrations and interference. Thin rubber layers have been added between the stiffened wing and the steel-wire tubes, as well as at the joints where the tubes attach to the nozzle lip, to further dampen vibrations.

The structure is mounted so that the propeller is positioned downstream of the nozzle exit at a distance $l_2 = 0.40$ m. The propeller APC 9 × 6, which has a diameter of 9″ (0.229 m) and a pitch of 6″ (0.152 m), has been used as a reference to design the propeller of the present investigation. This has been obtained by scaling the diameter to $D = 0.30$ m and reshaping the blade sections to a NACA-4412 profile, except for the first 0.01 m, which features an elliptical section. Figure 3 reports the chord and twist angle distributions of the blade. Further details on the design of the propeller can be found in Grande *et al.* (2022b).

The nacelle contains the motor driving the propeller, a Lehner Motors LMT 2280/34 brushless inrunner (LMT 2280 Brushless Inrunner Motor, Lehner Motoren Technik GmbH, Hohenbrunn, Bavaria, Germany). It features 2280 windings, which results in a motor velocity constant K_v of

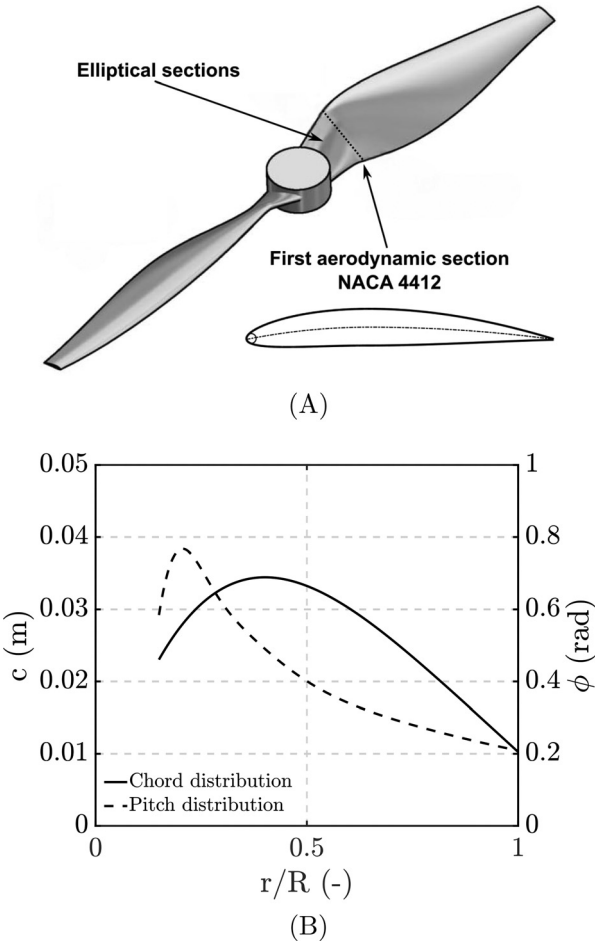

FIG. 3. (A) 3D model of the two-bladed propeller, (B) chord and pitch angle distributions.

218 RPM V^{-1}. This constant defines how many revolutions per minute (RPM) the motor turns per volt of applied voltage under no-load conditions. The motor is controlled by a trapezoidal electronic speed controller (ESC) that operates using pulse width modulation (PWM) and is powered by an external programmable 5 kW direct current (DC) power source.

Three different rotational speeds, i.e., 4000, 6000, and 8000 RPM, have been investigated to validate the proposed methodology. Calculating the advance ratio as $J = W_\infty/n\mathrm{D}$, with n being the propeller rotational frequency in hertz, the resulting values correspond to $J = 0.45$, $J = 0.30$, and $J = 0.23$, respectively.

1. Acoustic measurements

A directivity arc, equipped with ten G.R.A.S. 40PH analog free-field microphones (GRAS 40PH-10 CCP Free-field Array Microphone, G.R.A.S. Sound & Vibration A/S, Holte, Denmark), has been used to take acoustic measurements. The microphones have a diameter of 7 mm, a frequency range between 10 and 20 kHz, and a maximum sound pressure level (SPL) of 135 dB. The arc has a radius of 1.5 m, but the microphones have been placed at $R_{\mathrm{mic}} = 1.3$ m from the rotor hub. The angular positions of the ten microphones

https://doi.org/10.1121/10.0037185

are referenced to the rotor axis, as illustrated in Fig. 2. Microphone 1 is positioned at 60°, oriented upstream with respect to the rotor plane, while microphone 10 is located at 150°. The angular spacing between two adjacent microphones is $\Delta\theta_{mic} = 10°$.

The calibration of the microphones has been performed using a G.R.A.S. 42AA pistonphone (GRAS 42AA Pistonphone, Class 1, G.R.A.S. Sound & Vibration A/S, Holte, Denmark.) with a calibration level of 114 dB and a reference sound pressure of 20 μPa. A National Instrument PXIe-4499 (PXIe-4499 High-Channel Count Sound and Vibration Module, National Instruments Corporation, Austin, TX) has been used to acquire the acoustic data and the encoder signal. The signals measured by the microphones have been recorded for 60 s at a sampling frequency of 51.2 kHz. Finally, Welch's method has been applied with a Hanning window characterized by a 50% overlap to obtain power spectral densities (PSDs) with a frequency resolution of 100 Hz.

2. Aerodynamic measurements

The flow approaching the propeller has been characterized by hot-wire anemometry (HWA). The fluctuations measured using this technique are primarily aligned with the mean velocity (Zamponi *et al.*, 2020), which, in this case, corresponds to the axial direction. Flow velocity has been measured on a point grid of eight streamwise positions and nine radial positions, as shown in Fig. 4. The probe, a platinum-plated tungsten wire 5 μm–wide and 1.25 mm–long, is a Dantec Dynamics P11 (P11 Hot-Wire Probe, Dantec Dynamics A/S, Skovlunde, Denmark) ($R_{20} = 3.4$, $R_l = 0.5$, $\alpha_{20} = 0.36$) operated using a constant temperature bridge and is mounted on a remotely operated 2D traversing system. Measurements are performed at a sampling frequency of 51.2 kHz for 60 s. The same parameters for Welch's method as in the aeroacoustic measurements have been applied to process the HWA data.

3. Test matrix

The investigated cases are summarized in the test matrix of Table I. Acoustic measurements have been taken for all configurations, for a total of 14 cases considering that three different RPM values are taken into account for each flow condition. Conversely, HWA measurements have been performed only for the configuration without the propeller in order to characterize the turbulent inflow at the nozzle exit and in the propeller case at 6000 RPM, considered the baseline one. The configurations where aerodynamic measurements are available are indicated with a colored cell in the table.

B. Amiet's model for rotors

A quick overview of Amiet's model for the low-fidelity prediction of TIN in the formulation accounting for B2B correlation is presented here. The reader is referred to Amiet (1976, 1989) for a more detailed formulation.

Figure 5 reports a sketch of the rotor problem, together with the most important quantities and parameters. The fixed reference frame $\mathbf{x}_0$ is centered at the rotor hub. The x–y plane lies in the rotor plane, while z corresponds to the axial direction, along which the free-stream velocity W_∞ is directed. The listener position is identified with the distance R_0 from the rotor hub and the elevation angle θ, taken with respect to the upstream direction of the z axis. The azimuthal angle $\gamma = \Omega t$ measures the instantaneous angular distance of the blade from the x axis.

For consistency with Amiet's notation, velocities are expressed in terms of Mach numbers. The axial Mach number is indicated with M_z, while, considering a blade element

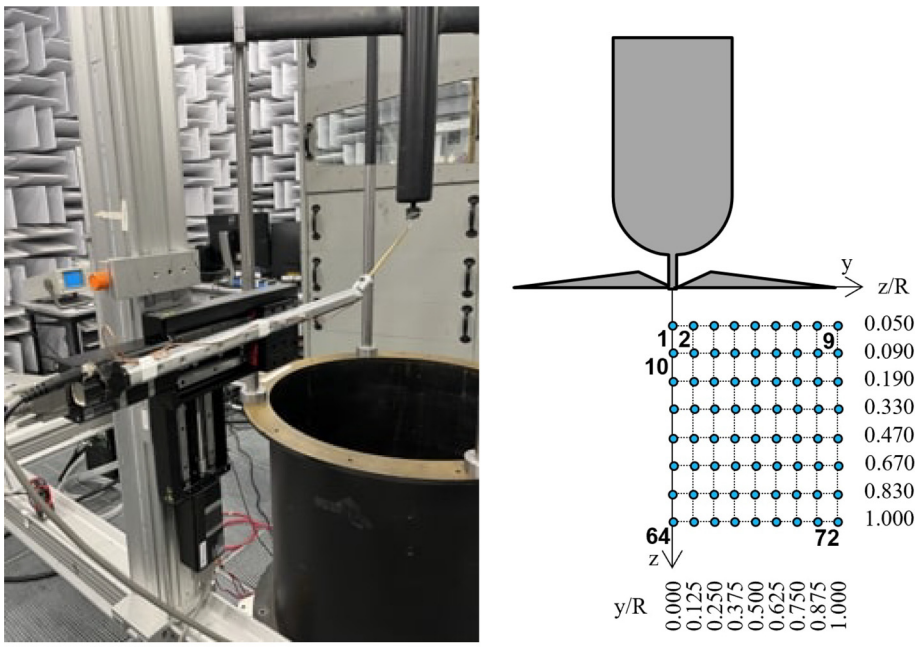

FIG. 4. (A) HWA setup, (B) HWA locations. Axial (streamwise) and radial (crosswise) distances are reported in terms of the propeller radius R.

TABLE I. Experimental test matrix. The free-stream velocity was kept constant at 9.5 ms^{-1}, meaning that the advance ratios at the three rotational speeds considered are $J = 0.45$, $J = 0.30$, and $J = 0.23$, respectively. Colored cells indicate cases where HWA measurements are available.

			Rotational speed (RPM)			
Grid	Motor	Propeller	4000	6000	8000	Description
Off	Off					Background noise (clean)
	On	Off	•	•	•	Background noise (clean) + motor
		On	•	•	•	Propeller noise with clean inflow
On	Off					Background noise (turbulent)
	On	Off	•	•	•	Background noise (turbulent) + motor
		On	•	•	•	Propeller noise with turbulent inflow

at a distance r from the rotor hub, the tangential (or azimuthal) Mach number $M_t = \Omega r/c_\infty$ is obtained. With respect to the fixed reference frame, this is indicated in vectorial form as

$$\mathbf{M}_t = (-M_t \sin\gamma, M_t \cos\gamma, 0). \tag{1}$$

In the most general configuration, the rotor is assumed to interact with a transverse velocity in its plane, characterized by a Mach number M_f. The angle between this velocity and the y axis, fixed relative to the rotor, is denoted as ψ. Both M_f and ψ are equal to zero in the present investigation but are kept in the formulation to keep the generality of the discussion. Taking into account these velocities, the blade element at a distance r, simplified in Amiet's theory into a flat plate with no radial pitch distribution, interacts with a velocity U_b directed along the chord direction, with Mach number indicated as M_b (see the details of Fig. 5), calculated as

$$M_b = \sqrt{M_z^2 + (M_t + M_f \cos(\gamma + \psi))^2}. \tag{2}$$

This velocity forms an angle α with the rotor plane, obtained as

$$\alpha = \arccos\left(\frac{M_z}{M_t + M_f \cos(\gamma + \psi)}\right). \tag{3}$$

Following the approach of Sinayoko *et al.* (2013), the present implementation of the model accounts for the radial pitch distribution $\phi(r)$. The velocity along the blade direction is thus given by $U_x = U_b \cos\delta$ and the corresponding Mach number is denoted as M_x. Here, $\delta = \alpha - \phi$ represents the angle between U_b and the chord direction, as shown in the detail of Fig. 5.

The motion of the blade, and hence the relative position of the sound source with respect to the listener, must be accounted for to correctly retrieve the noise prediction. In the fixed reference frame, the listener position is identified by

$$\begin{cases} x_0 = R_0 \sin\theta, \\ y_0 = 0, \\ z_0 = R_0 \cos\theta. \end{cases} \tag{4}$$

This position must be expressed in terms of the moving reference frame associated with the blade rotation, taking into account also the retarded source position of the airfoil segment, i.e., the position where the source is when the acoustic wave reaches the listener. This is indicated with $\mathbf{x}_s$ and is expressed by

$$\begin{cases} x_s = -M_f r_e \sin\psi, \\ y_s = -M_f r_e \cos\psi, \\ z_s = -M_z r_e, \end{cases} \tag{5}$$

with r_e being the distance of the listener from the retarded source derived as

$$r_e = R_0 \frac{M_s \cos\Lambda + \sqrt{1 - M_s^2 \sin^2\Lambda}}{1 - M_s^2}. \tag{6}$$

$M_s = \sqrt{M_f^2 + M_z^2}$ is the convection Mach number and Λ is the angle between $\mathbf{M}_s$ and $\mathbf{x}_0$,

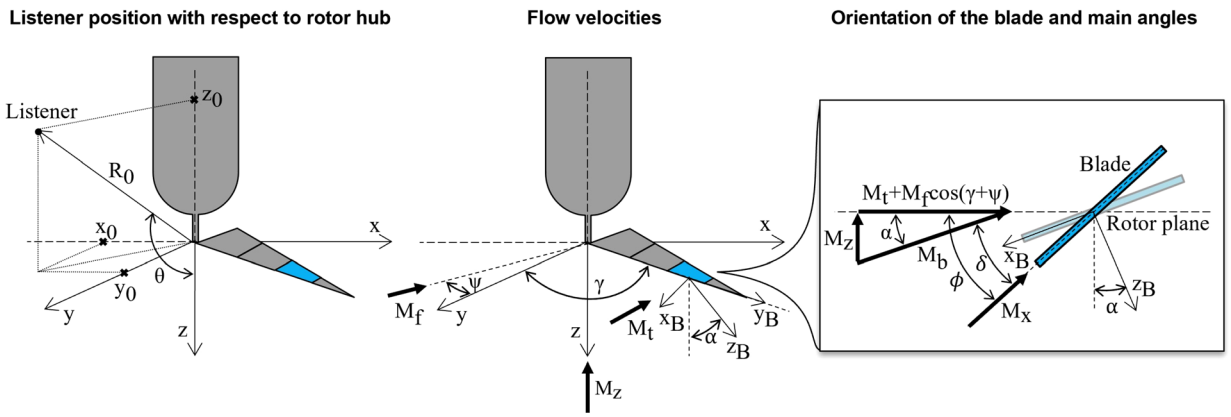

FIG. 5. Rotor problem with key parameters and quantities.

https://doi.org/10.1121/10.0037185

$$\Lambda = \arccos\left(\frac{M_f \sin\psi \sin\theta + M_z \cos\theta}{M_s}\right). \tag{7}$$

The "present" source position $\mathbf{x}_\mathrm{p}$ must then be determined. This corresponds to the position of the source as if it had moved in the chordwise direction during the time taken by the acoustic wave to travel from its emission point identified by $\mathbf{x}_\mathrm{s}$ to the listener. Amiet (1989) shows that $\mathbf{x}_\mathrm{p}$ reads as

$$\begin{cases} x_p = r_e[-(M_t \sin\gamma + M_f \cos\gamma \sin(\gamma+\psi))], \\ y_p = r_e[M_t \cos\gamma - M_f \sin\gamma \sin(\gamma+\psi)], \\ z_p = 0. \end{cases} \tag{8}$$

With respect to $\mathbf{x}_\mathrm{p}$, the listener will be identified by $\mathbf{x}_0 - \mathbf{x}_\mathrm{p}$. Accounting for the rotation around the z axis to consider the azimuthal rotation $(\pi/2 - \gamma)$ with a rotation matrix R_z,

$$\mathsf{R}_z = \begin{bmatrix} \cos\left(\frac{\pi}{2}-\gamma\right) & -\sin\left(\frac{\pi}{2}-\gamma\right) & 0 \\ \sin\left(\frac{\pi}{2}-\gamma\right) & \cos\left(\frac{\pi}{2}-\gamma\right) & 0 \\ 0 & 0 & 1 \end{bmatrix}, \tag{9}$$

and for the angle α formed by the blade with respect to the rotor plane with a rotation matrix R_y,

$$\mathsf{R}_y = \begin{bmatrix} \cos\alpha & 0 & -\sin\alpha \\ 0 & 1 & 0 \\ \sin\alpha & 0 & \cos\alpha \end{bmatrix} \tag{10}$$

[as in the formulation of Sinayoko *et al.* (2013)], the position of the listener $\mathbf{x}_\mathrm{B}$ in the blade reference frame (from which the subscript $_\mathrm{B}$) is finally obtained as

$$\mathbf{x}_\mathrm{B} = \mathsf{R}_y \mathsf{R}_z (\mathbf{x}_0 - \mathbf{x}_\mathrm{p}), \tag{11}$$

resulting in

$$\begin{cases} x_\mathrm{B} = [(x_0 - x_\mathrm{p})\sin\gamma - (y_0 - y_\mathrm{p})\cos\gamma]\cos\alpha - (z_0 - z_\mathrm{p})\sin\alpha; \\ y_\mathrm{B} = (x_0 - x_\mathrm{p})\cos\gamma + (y_0 - y_\mathrm{p})\sin\gamma; \\ z_\mathrm{B} = [(x_0 - x_\mathrm{p})\sin\gamma - (y_0 - y_\mathrm{p})\cos\gamma]\sin\alpha + (z_0 - z_\mathrm{p})\cos\alpha. \end{cases} \tag{12}$$

Once the motion of the sound source is taken into account, Amiet (1976) treats the sound produced by each rotating blade at a certain azimuthal position as if it was generated in rectilinear motion, enabling the application of the analytical model (Amiet, 1975) to the rotating regime. This procedure relies on a fundamental assumption: the frequency range of the noise is much higher than the rotational speed of the rotor.

The far-field acoustic pressure $S_{pp}(\mathbf{x}_\mathrm{B}, \omega_0)$ at the listener position $\mathbf{x}_\mathrm{B} = (x_\mathrm{B}, y_\mathrm{B}, z_\mathrm{B})$, with $\omega_0 = 2\pi f$ being the sound frequency as heard by the observer in the fixed reference frame, is hence retrieved through the azimuthal average of the instantaneous noise emission $S'_{pp}(\mathbf{x}_\mathrm{B}, \omega_0, \gamma)$ through

$$S_{pp}(\mathbf{x}_\mathrm{B}, \omega_0) = \frac{1}{2\pi}\int_0^{2\pi} \left(\frac{\omega_\mathrm{B}}{\omega_0}\right) S'_{pp}(\mathbf{x}_\mathrm{B}, \omega_0, \gamma)\mathrm{d}\gamma. \tag{13}$$

$\omega_\mathrm{B}/\omega_0$ describes the Doppler's effect due to the sound source motion with respect to the listener position. This is calculated as

$$\frac{\omega_0}{\omega_\mathrm{B}} = 1 + \frac{\mathbf{M}_t \cdot \hat{\mathbf{s}}}{1 - \mathbf{M}_r \cdot \hat{\mathbf{s}}},$$

with $\mathbf{M}_\mathrm{r}$ representing the Mach number of the source with respect to the fluid, expressed in vectorial form as

$$\mathbf{M}_\mathrm{r} = (M_\mathrm{f}\sin\psi - M_\mathrm{t}\sin\gamma, M_\mathrm{f}\cos\psi + M_\mathrm{t}\cos\gamma, M_z), \tag{14}$$

$\hat{\mathbf{s}}$ being the unit vector from the retarded source position to the listener according to

$$\hat{\mathbf{s}} = \left(\frac{x_s - x_0}{r_e}, \frac{y_s - y_0}{r_e}, \frac{z_s - z_0}{r_e}\right). \tag{15}$$

$S'_{pp}(\mathbf{x}_\mathrm{B}, \omega_0, \gamma)$, expressed in terms of the Doppler-shifted frequency as heard by the listener ω_0, is related to $S_{pp}(\mathbf{x}_\mathrm{B}, \omega_\mathrm{B}, \gamma)$, depending on the angular frequency of the blade forces ω_B through

$$S'_{pp}(\mathbf{x}_\mathrm{B}, \omega_0, \gamma) = \frac{\omega_\mathrm{B}}{\omega_0} S_{pp}(\mathbf{x}_\mathrm{B}, \omega_\mathrm{B}, \gamma), \tag{16}$$

meaning that a factor $(\omega_\mathrm{B}/\omega_0)^2$ will appear in Eq. (16).

In the formulation accounting for the correlation of the unsteady surface pressure induced by the chopping of an eddie by more than one blade, $S_{pp}(\mathbf{x}_\mathrm{B}, \omega_\mathrm{B}, \gamma)$ takes the form

$$S_{pp}(\mathbf{x}_\mathrm{B}, \omega_\mathrm{B}, \gamma) = G|\mathcal{L}(K_x, K_y, M_x)|^2 \times \sum_{n=-\infty}^{\infty} \Phi_{ww}\left(K_x, K_y, K_z^{(n)}\right) \frac{2\pi}{\left(\frac{c}{2}\right)^2 \overline{w'^2} Z}, \tag{17}$$

with

$$G = \left(\frac{\omega_\mathrm{B} z_\mathrm{B} \rho_0 c}{2 c_0 \sigma^2}\right)^2 \pi U_\mathrm{x} \left(\frac{L}{2}\right) \overline{w'^2} \left(\frac{c}{2}\right)^2. \tag{18}$$

ρ_0 indicates the flow density and c_0 is the speed of sound. The blade geometry is represented by the chord c and the span L, while the convection effects are accounted for through $\sigma_0 = \sqrt{x_\mathrm{B}^2 + \beta_x^2(y_\mathrm{B}^2 + z_\mathrm{B}^2)}$, with $\beta_x = \sqrt{1 - M_x^2}$. $\mathcal{L}(K_x, K_y, M_x)$ is the aeroacoustic transfer function, for which the original formulation of Amiet (1989) has been used, while $\Phi_{ww}(K_x, K_y, K_z^{(n)})$ is the 3D turbulence spectrum. The wavenumbers are calculated as

$$\begin{cases} K_x = \dfrac{\omega_B}{U_x}, \\ K_y = \dfrac{\omega_B y_B}{c_0 \sigma}, \\ K_z^{(n)} = \dfrac{2\pi n + \omega_0 T_2}{Z}. \end{cases} \tag{19}$$

K_x takes this form under the hypothesis of frozen turbulence, while K_y under the large-span wing assumption, i.e., $M_\infty\ K_x\ L/2 \gg 0$, and $K_z^{(n)}$ is obtained in the framework of the B2B correlation. The latter term features the Doppler-shifted frequency ω_0, the time between consecutive chops of a certain eddy as heard by the listener T_2, and the distance Z, which represents the distance between the path of two adjacent blades measured with respect to the fluid, nZ thus being the distance between the zeroth and the nth blade paths. T_2 is calculated by adding a $\Delta\tau$ to the time between eddie chops T_1 through

$$T_2 = T_1 + \Delta\tau. \tag{20}$$

The expression for T_1 reads

$$T_1 = T_t \left(\frac{V_t}{V_z}\right) \sin\alpha \cos\alpha, \tag{21}$$

where $T_t = 2\pi/\Omega B$, while $\Delta\tau$ is calculated as

$$\Delta\tau = X \left(\frac{M_x - \dfrac{x_B}{\sigma_0}}{\beta_x^2 c_\infty} \right) + Y \frac{y_B}{c_\infty \sigma_0}, \tag{22}$$

with $X = (T_t - T_1)\ V_t, Y = T_1\ V_f\ \sin(\gamma + \psi)$. The distance Z is calculated as $Z = T_t\ V_t\ \sin\alpha$. The reader is referred to Amiet (1976, 1989) for the physical meaning of these parameters and the derivation of the respective expressions, whose explanation is beyond the scope of this study.

III. AMIET'S MODEL MODIFICATION

A. Analytical formulation

The modification of Amiet's model proposed in the present study consists of converting the 3D spectrum $\Phi_{ww}(K_x, K_y, K_z^{(n)})$ in Eq. (17) into a 1D one $\Theta_{ww}(K_x)$. This is achieved by applying a strip theory approach (Christophe *et al.*, 2009), which models the noise produced by a blade of span L as the summation of the noise contributions generated by M narrow spanwise portions of the blade, referred to as *strips*. The present procedure implements the theory in its inverse formulation, as done by Kücükcoskun (2012), in which the noise emitted by a blade strip is calculated as the difference of the sound produced by two very large-span blades whose difference in width is equal to the strip width L/M itself, as shown in the conceptual sketch of the inverse strip theory approach reported in Fig. 6. For the present case, this is expressed considering $S'_{pp}(\mathbf{x}_B, \omega_0, \gamma)$ as the noise emitted by the strip m, which is therefore obtained through

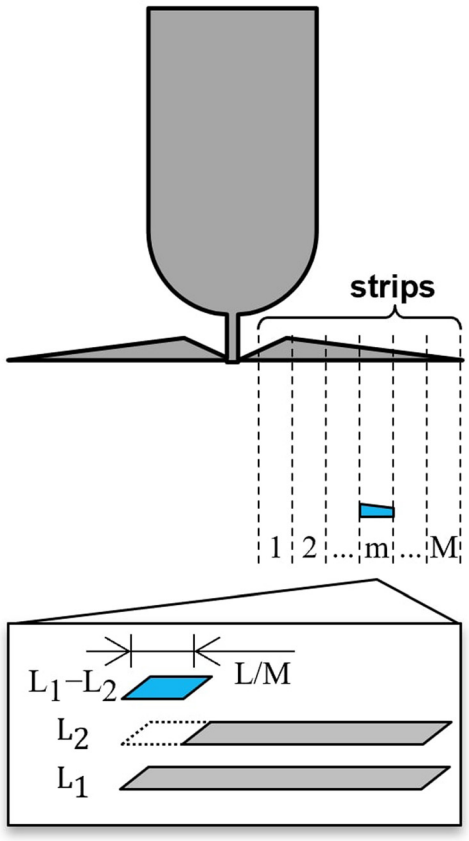

FIG. 6. Sketch of the application of the inverse strip theory approach for the calculation of the blade instantaneous sound emission.

$$S'_{pp}(\mathbf{x}_B, \omega_0, \gamma)|_m = \left(S'_{pp}(\mathbf{x}_B, \omega_0, \gamma)|_{L_1} - S'_{pp}(\mathbf{x}_B, \omega_0, \gamma)|_{L_2} \right)\Big|_m, \tag{23}$$

with $L_1 - L_2 = L/M$ and $L_1, L_2 \to \infty$.

The overall noise produced is hence computed by applying Amiet's model M times, one for each blade considering local inflow conditions. By using Eqs. (16) and (17), all the contributions are summed through

$$S_{pp}(\mathbf{x}_B, \omega_0) = B \sum_{m=1}^{M} S_{pp}(\mathbf{x}_B, \omega_0)\Big|_m, \tag{24}$$

with B indicating the number of blades. The application of the inverse strip theory does not involve any assumption or modification of the turbulence term: the analytical spectrum selected to describe the inflow will be scaled through the local turbulence characteristics, regardless of its form.

The substitution of $\Phi_{ww}(K_x, K_y, K_z^{(n)})$ with $\Theta_{ww}(K_x)$ in Eq. (17) can be carried out considering the work of Wilson (1997), who calculated the 3D correlations and spectral functions in the case of homogeneous isotropic turbulence. Indeed, considering a generic 3D reference system x, y, and z with corresponding wavenumbers k_x, k_y, and k_z, the 3D turbulence spectrum of the w velocity component $\Phi_{ww}(k_x, k_y, k_z)$ is obtained as the Fourier transform with

https://doi.org/10.1121/10.0037185

respect to k_z of the two-dimensional (2D) cross-spectrum $R_{ww}(k_x, k_y; z)$,

$$\Phi_{ww}(k_x, k_y, k_z) = \frac{1}{2\pi}\int_{-\infty}^{+\infty} R_{ww}(k_x, k_y; z)\mathrm{e}^{-\mathrm{i}zk_z}\mathrm{d}k_z. \tag{25}$$

Starting from the analytical expression of Φ_{ww}, valid in the case of homogeneous isotropic turbulence, Wilson (1997) explicitly calculated $R_{ww}(k_x, k_y; z)$ as

$$R_{ww}(k_x, k_y; z) = \frac{\overline{u'^2}k_h^2 L_{ww}^4 \zeta_h^{\nu+2}}{\pi 2^{\nu+1}\Gamma(\nu)\left(1 + k_h^2 L_{ww}^2\right)^{\nu+2}}\mathcal{B}_{\nu+2}(\zeta_h), \tag{26}$$

with $k_h^2 = k_x^2 + k_y^2$, $\zeta_h = (z/L_{ww})\sqrt{1 + k_h^2 L_{ww}^2}$, $\mathcal{B}_{\nu+2}$ being the Bessel's function of the second kind of order $\nu + 2$, and ν setting the generic power law dependence in the inertial subrange. For simplicity, the superscript z in the integral length scale L_{ww}^z has been omitted.

For $z = 0$, $R_{ww}(k_x, k_y; z)$ can be seen as the 2D wavenumber spectrum $\Psi_{ww}(k_x, k_y)$, and Eq. (26) simplifies into

$$\Psi_{ww}(k_x, k_y) = \frac{\nu(\nu+1)\overline{u'^2}k_h^2 L_{ww}^4}{\pi\left(1 + k_h^2 L_{ww}^2\right)^{\nu+2}}. \tag{27}$$

Using Eq. (27), Eq. (26) can be rewritten as

$$\begin{aligned} R_{ww}(k_x,k_y;z) &= \left[\frac{1}{\nu(\nu+1)}\frac{\zeta_h^{\nu+2}}{2^{\nu+1}\Gamma(\nu)}\mathcal{B}_{\nu+2}(\zeta_h)\right]\Psi_{ww}(k_x,k_y) \\ &= A(k_x,k_y;z)\Psi_{ww}(k_x,k_y), \end{aligned} \tag{28}$$

with the auxiliary function $A(k_x, k_y; z)$ introduced to indicate the terms in square brackets.

This relationship between the 2D cross-spectrum and the 2D wavenumber spectrum [Eq. (28)] can be used to modify the turbulence term of Eq. (17). Indeed, it is possible to write

$$\begin{aligned} \Phi_{ww}\left(K_x,K_y,K_z^{(n)}\right) &= \mathcal{F}\left\{R_{ww}\left(K_x,K_y;Z^{(n)}\right)\right\} \\ &= \frac{1}{2\pi}\int_{-\infty}^{\infty} R_{ww}\left(K_x,K_y;Z^{(n)}\right)\mathrm{e}^{-\mathrm{i}Z^{(n)}K_z^{(n)}}\mathrm{d}K_z^{(n)}, \end{aligned} \tag{29}$$

with $Z^{(n)}$ indicating a fictitious spatial coordinate corresponding to the wavenumber $K_z^{(n)}$ and F representing the Fourier transform operator. By applying Eq. (28) to the present case and moving the 2D wavenumber spectrum outside the Fourier transform operator, it follows that

$$\begin{aligned} \Phi_{ww}\left(K_x,K_y,K_z^{(n)}\right) &= \mathcal{F}\left\{A\left(K_x,K_y;Z^{(n)}\right)\Psi_{ww}(K_x,K_y)\right\} \\ &= \Psi_{ww}(K_x,K_y)\tilde{A}\left(K_x,K_y,K_z^{(n)}\right), \end{aligned} \tag{30}$$

with A indicating the auxiliary function allowing the conversion of the turbulence term from 3D to 2D and $\tilde{A}$ its Fourier transform. However, rather than performing the Fourier transform of A, $\tilde{A}$ can be conveniently obtained as

$$\tilde{A}\left(K_x,K_y,K_z^{(n)}\right) = \frac{\Phi_{ww}\left(K_x,K_y,K_z^{(n)}\right)}{\Psi_{ww}(K_x,K_y)}, \tag{31}$$

considering that, under the assumption of homogeneous isotropic turbulence, analytical expressions exist for Φ_{ww} and Ψ_{ww}. Since any axial dependence has now been removed from the turbulence velocity spectrum, the auxiliary function $\tilde{A}(K_x, K_y, K_z^{(n)})$ can be defined as *axial correlation length*.

Owing to von Kármán's assumptions and framework for homogeneous isotropic turbulence (von Kármán, 1948), ν is finally considered equal to $1/3$, resulting in Kolmogorov's $-5/3$ power law, and the three-wavenumber spectrum of the upwash velocity component with respect to the blade, i.e., corresponding to the axial velocity component in the present reference frame, reads

$$\Phi_{ww}(k_x, k_y, k_z) = \frac{E(k)}{4\pi k^2}\left(1 - \frac{k_z^2}{k^2}\right), \tag{32}$$

with

$$E(k) = \frac{55}{9\sqrt{\pi}}\frac{\Gamma(5/6)}{\Gamma(1/3)}\frac{\overline{w'^2}}{k_e}\frac{k}{\left[1 + \left(\frac{k}{k_e}\right)^2\right]^{17/6}}. \tag{33}$$

The expression of the two-wavenumber spectrum of the same velocity component is then

$$\Psi_{ww}(k_x, k_y) = \frac{4}{9\pi}\frac{\overline{w'^2}}{k_e^2}\frac{\left(\frac{k_x}{k_e}\right)^2 + \left(\frac{k_y}{k_e}\right)^2}{\left[1 + \left(\frac{k_x}{k_e}\right)^2 + \left(\frac{k_y}{k_e}\right)^2\right]^{7/3}}, \tag{34}$$

leading to the following expression for $\tilde{A}(K_x, K_y, K_z^{(n)})$:

$$\tilde{A}\left(K_x,K_y,K_z^{(n)}\right) = \left(\frac{55}{16}\frac{L_{ww}}{\pi}\right)\frac{\left(1 + \hat{k}_h^2\right)^{7/3}}{\left(1 + \hat{k}^2\right)^{17/6}}. \tag{35}$$

The last step consists of turning the 2D wavenumber spectrum Ψ_{ww} into the product of a 1D spectrum Θ_{ww} and another auxiliary function. This has been done by Amiet (1975) for his formulation for an airfoil in rectilinear motion under the assumption of large span. This is a reasonable assumption considering that the inverse approach of the strip theory considers the sound as produced by an airfoil of infinite span. It is hence possible to write

$$\Psi_{ww}(K_x, K_y) = \frac{1}{\pi}\Theta_{ww}(K_x)l_y(K_x), \tag{36}$$

with $l_y(K_x)$ being the spanwise coherence length of the upwash velocity component, for which Amiet (1975) proposes the following expression:

$$l_y(K_x) = \frac{8L_{ww}^z}{3}\left[\frac{\Gamma(1/3)}{\Gamma(5/6)}\right]^2 \frac{\hat{K}_z^2}{\left(3+8\hat{K}_z^2\right)\sqrt{1+\hat{K}_x^2}}. \quad (37)$$

This formulation, which incorporates the 1D turbulence term and the spanwise coherence length, is valid for a listener positioned in the midspan plane of a blade in rectilinear motion. However, as will be shown in Sec. III B, this modification does not impact the accuracy of noise directivity compared to the canonical implementation of Amiet's model.

The introduction of the axial correlation length $\tilde{A}(K_x, K_y, K_z^{(n)})$ and the spanwise coherence length $l_y(K_x)$ allows hence the turbulence term to be expressed in terms of the 1D spectrum $\Theta_{ww}(K_x)$, finally converting Eq. (17) (applied to the mth strip) into

$$S_{pp}(\mathbf{x}_B, \omega_B, \gamma)|_m = G|\mathcal{L}(K_x, K_y, M_x)|^2 \left(\frac{1}{\pi}\Theta_{ww}(K_x) l_y(K_x)\right) \times \sum_{n=-\infty}^{\infty} \tilde{A}\left(K_x, K_y, K_z^{(n)}\right) \frac{2\pi}{\left(\frac{c}{2}\right)^2 \overline{w'^2} Z}. \quad (38)$$

The 1D spectrum can be modeled using a von Kármán spectrum

$$\Theta_{ww}(K_x) = \frac{2}{27\sqrt{\pi}} \frac{\Gamma(5/6)}{\Gamma(7/3)} \frac{\overline{w'^2}}{k_e} \frac{3+8(K_x/k_e)^2}{[1+(K_x/k_e)^2]^{11/6}}, \quad (39)$$

with $k_e = \sqrt{\pi}/L_{ww}^z \Gamma(5/6)/\Gamma(1/3)$. This implementation, whose validation is presented in Sec. III B, only requires the knowledge of the turbulence intensity, free-stream velocity, and integral length scale. Alternatively, it is possible to use a direct probe measurement in the frequency domain as input, such as that obtained by means of HWA, as in Sec. III C.

B. Validation with experimental data

The proposed modification is validated using experimental acoustic measurements. Amiet's model has been applied using the radial distribution of flow characteristics sampled far upstream at the nozzle exit in the configuration without the propeller (see Sec. II A). Comparisons between the predictions and the measurements are reported in terms of SPL in Fig. 7 for 4000, 6000, and 8000 RPM, respectively. For each case, experimental measurements with both turbulent and clean inflow are presented, with listener positions considered at 60° and 130°. Background noise, omitted from the figures for clarity, was verified to be well below the propeller noise levels in both inflow cases.

Amiet's model has been implemented in two formulations featuring the 3D turbulence spectrum Φ_{ww} and the 1D one Θ_{ww}. These have been modeled using the von Kármán expressions given in Eqs. (32) and (39), respectively. Both have been applied with the inverse strip theory approach, retaining the B2B correlation modeling. This comparison allows possible effects resulting from the modification of the turbulence term to be identified.

TIN dominates the sound spectra in the low- and mid-frequency range, approximately up to the 20th–30th BPF (Paterson and Amiet, 1982), as can be seen from the cases at 4000 and 6000 RPM with respect to the clean inflow configuration. At higher frequencies, up to the 100th BPF, the spectra feature a clear bump with tones concentrated between the 40th and the 70th BPF. These are clearly caused by the propeller motor, as indicated in the plots with an arrow, while the bump can likely be attributed to the blade self-noise and laminar separation (Grande *et al.*, 2022a; Casalino *et al.*, 2022). The bump in the high-frequency range can hardly be recognized for the case at 8000 RPM, as the noise levels related to TIN increase significantly in this rotation regime.

In general, the acoustic spectra exhibit clear signs of reflections, most likely originating from the nozzle, nacelle, or support rig. These reflections primarily affect the high-frequency range beyond the 10th BPF, introducing "sawtooth" peaks in the spectra. These peaks, particularly evident for the listener position at 60° and marked in the plots with an arrow, should not be confused with the haystacking features in the low- and mid-frequency ranges. Indeed, here the far-field acoustic spectra exhibit distinct broadband characteristics along with quasi-tonal peaks resulting from the B2B correlation. As expected, the prominence of these narrow peaks and the frequency range over which they appear increase with rotational speed. This occurs because, at higher speeds, turbulent eddies are more likely to be chopped by multiple blades.

Regarding the low-fidelity prediction, the two formulations of Amiet's model retrieve nearly identical results at 4000. 6000, and 8000 RPM. Only a slight difference, seemingly proportional to the rotational speed, becomes noticeable at frequencies above the 10th BPF. Specifically, the curve corresponding to the original implementation of Amiet's model with the 3D turbulence spectrum lies slightly below that of the modified approach using the 1D spectrum. The match between the two formulations is confirmed by the directivity plots in Fig. 8. These show the overall sound pressure level (OASPL) calculated in the frequency range where TIN dominates [f = (0.1 BPF–30 BPF)]. Experimental measurements have not been included, as microphone data is dominated by other flow-induced noise sources in the angular range where TIN directivity decreases. As a result, these additional noise contributions would hinder a meaningful comparison.

The exact agreement between Amiet's model in its original formulation with the 3D spectrum and the modified approach using a 1D turbulence input serves as a validation of the proposed methodology. At the same time, both predictions closely match the experimental SPL, accurately capturing both the broadband and quasi-tonal components within the low-fidelity framework. The tonal peaks at BPF harmonics are not captured as the turbulence input term in

https://doi.org/10.1121/10.0037185

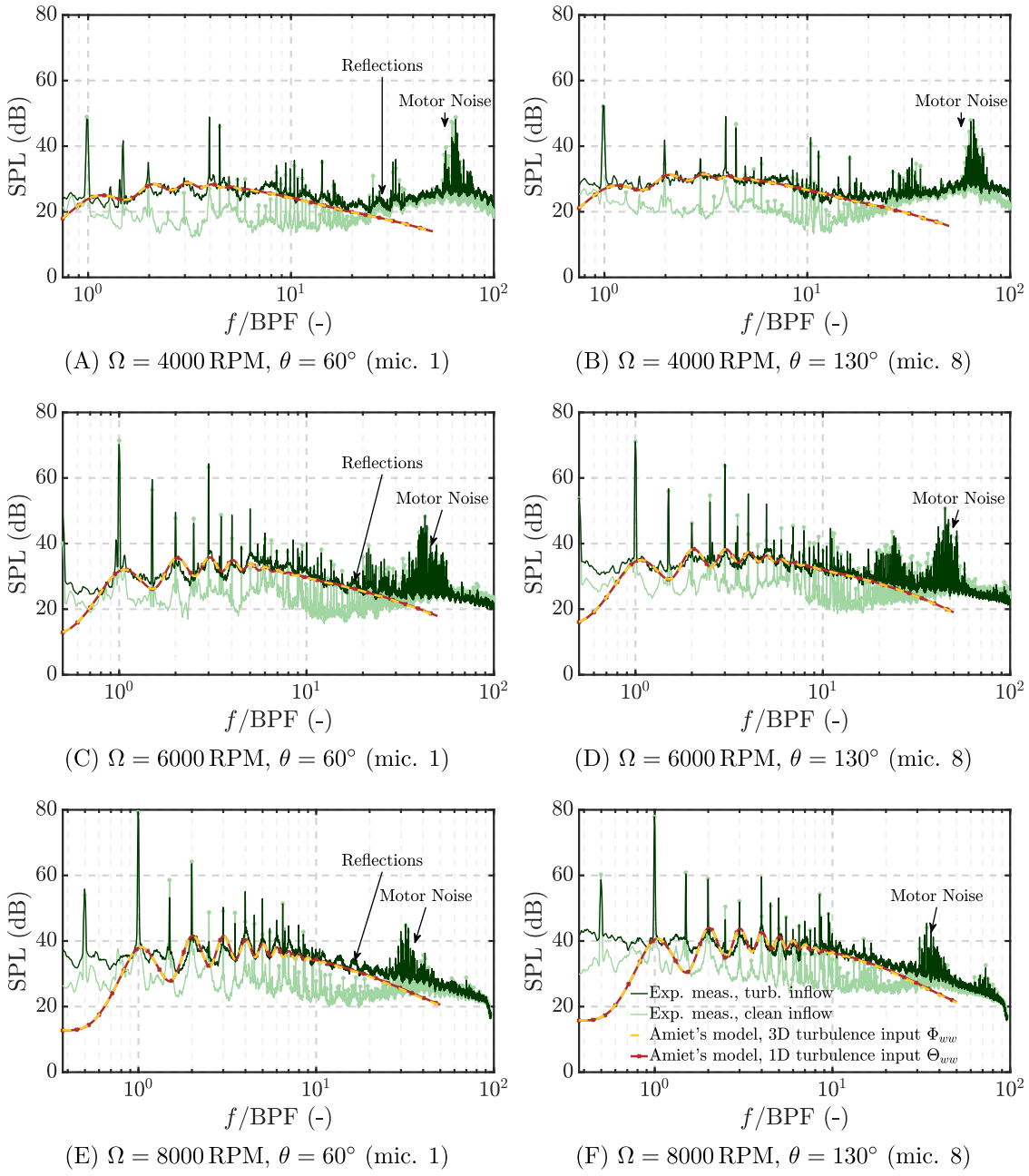

FIG. 7. Sound pressure level predicted by Amiet's model with 3D and 1D turbulence inputs compared to experimental measurements with turbulent and clean inflow at the three rotational speeds and at two different microphone positions. The reference pressure used to calculate the SPL is 2×10^{-5} Pa.

Amiet's model does not include the description of this contribution.

C. Application of the methodology with hot-wire measurements of the turbulent inflow as input

The formulation with the 1D turbulence term is applied for the case at 6000 RPM using the velocity frequency spectra obtained from the HWA measurements as input. The probe specifically measures velocity fluctuations in the axial direction, as explained in Sec. II A 2, which corresponds to the upwash component relative to the rotor plane. This velocity component is responsible for inducing unsteady loading on the blades, meaning that this measurement can be rightfully used as input in the low-fidelity model.

1. Turbulent inflow characterization

Figure 9 presents the radial distributions of the time-averaged velocity and the root mean square of the velocity component measured with HWA. The distributions sampled far upstream at $z/\mathrm{R} = 1.000$ (indicated in the figure also with "ups") are compared to those measured near the rotor plane at $z/\mathrm{R} = 0.050$ (indicated with "dws" which stands for "downstream"). For the latter, the root mean square is reported both for the original signal and after filtering out the tonal components caused by the blade passage. Filtering

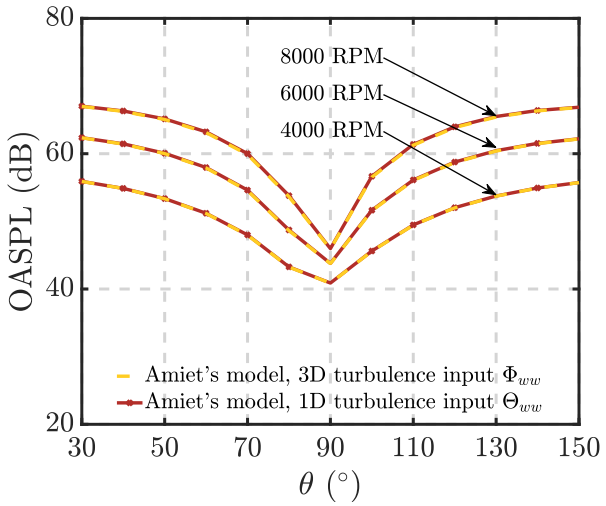

FIG. 8. Overall sound pressure level predicted by Amiet's model with 3D and 1D turbulence for the angular range $\theta = [30°, 150°]$ at 4000, 6000, and 8000 RPM. The reference pressure used to calculate the SPL is 2×10^{-5} Pa.

is performed using an in-house peak detection algorithm applied to the PSDs of the HWA signals.

While the time-averaged velocity increases relative to upstream conditions, the removal of tonal components reveals a slight decrease in axial velocity fluctuations compared to upstream conditions. This effect is due to the streamtube contraction, which, as it stretches the turbulent structures in the streamwise direction, causes a simultaneous reduction in the streamwise velocity fluctuation, similar to what occurs in the convergent section of a wind tunnel (Amiet *et al.*, 1990; Batchelor and Proudman, 1954).

Figure 10 compares the HWA velocity spectra for the two sampling positions along the axial direction and for two different radial positions: $y/\mathrm{R} = 0.500$ and $y/\mathrm{R} = 1.000$. The plot also presents the filtered HWA velocity spectra sampled at the rotor plane, with the tones removed.

The HWA spectra sampled close to the rotor plane present lower levels in the low-frequency range (approximately up to $f/\mathrm{BPF} \simeq 0.6$). This is especially evident at the central radial locations, whereas positions near the rotor axis and toward the blade tip exhibit upstream and downstream spectra that almost perfectly overlap. This behavior is attributed to the reduction in streamwise velocity fluctuations due to streamtube contraction, as observed in the root mean square variation. This variation can be calculated from the upstream conditions using RDT, as done by Majumdar and Peake (1998) and Simonich *et al.* (1986). An implementation of Goldstein's formulation (Goldstein, 1978) has been implemented here following the approach of Glegg and Devenport (2017) for the axisymmetric contraction, with the predicted altered spectra reported in Fig. 10 together with the HWA ones. Good agreement is observed between the RDT results and the experimental measurements at $z/\mathrm{R} = 0.050$, demonstrating how simple pointwise measurements can effectively describe the inflow conditions and their alteration. The impact of this alteration will become evident in the application of the modified Amiet's model using directly probe measurements as input.

2. Noise prediction

To correctly incorporate HWA measurements into the low-fidelity model, an appropriate conversion to a spatial wavenumber spectrum is required. This conversion relies on Taylor's hypothesis, which considers frozen turbulence, as also assumed by Amiet (1975, 1976). By assuming the convective velocity to be equal to the inflow velocity W_∞, the spectrum $\Theta_{ww}(K_x)$ used in Amiet's model can be derived from the experimental frequency spectrum through

$$\Theta_{ww}(K_x) = \frac{W_\infty}{2\pi}\Theta_{ww}(f)\Big|_{\mathrm{HW}}. \tag{40}$$

The advantage of using pointwise flow measurements as input is assessed by comparing the predictions obtained with the spectra sampled far upstream ($z/\mathrm{R} = 1.000$) and very close to the rotor plane ($z/\mathrm{R} = 0.050$), shown in Fig. 11. The modified Amiet's model has been implemented using the respective radial distributions of the time-average and root mean square of the axial velocity component shown in Fig. 9. The plot compares the low-fidelity predictions with the experimental acoustic measurements at the angular positions $\theta = 60°$ and $\theta = 130°$. An accurate result is

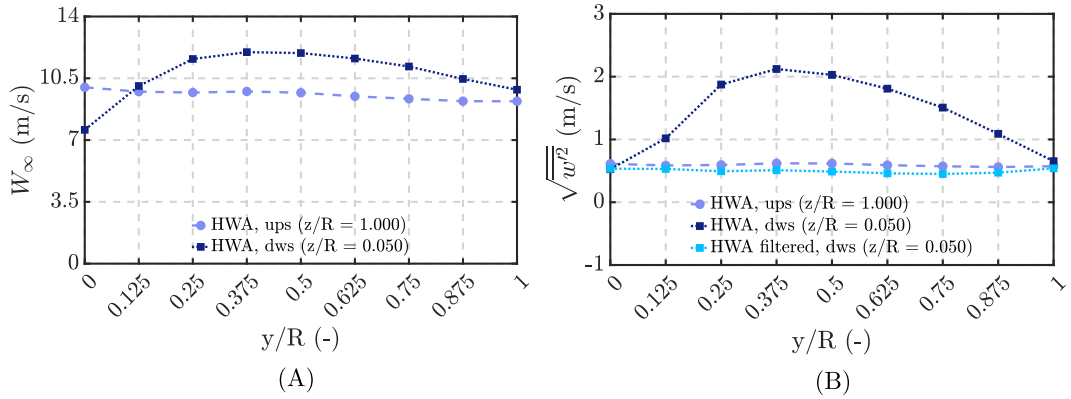

FIG. 9. Radial distributions far upstream at $z/\mathrm{R} = 1.000$ and near the rotor plane at $z/\mathrm{R} = 0.050$ (in the filtered and non-filtered cases) for the (A) time average, (B) root mean square of the axial velocity component measured using HWA.

https://doi.org/10.1121/10.0037185

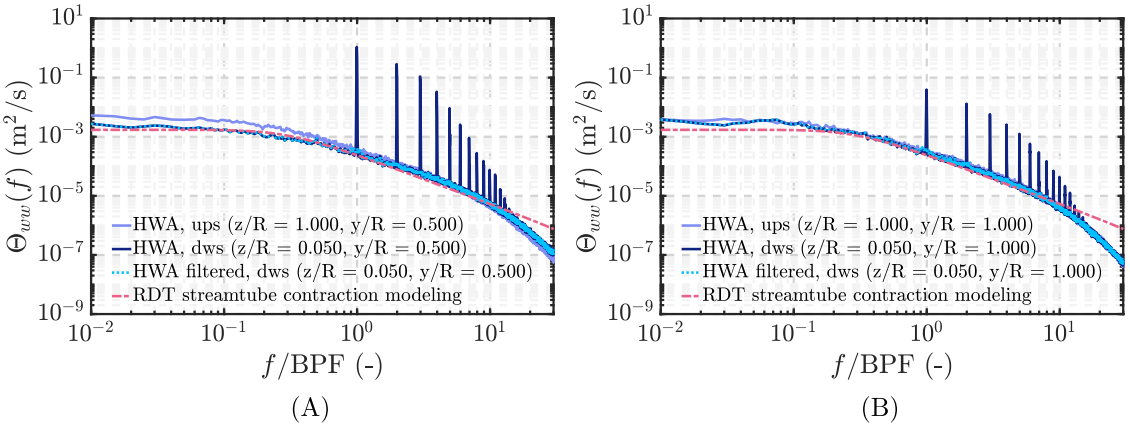

FIG. 10. Frequency spectra of the inflow velocity at the radial positions (A) $y/\mathrm{R} = 0.500$, (B) $y/\mathrm{R} = 1.000$. The spectra sampled far upstream at $z/\mathrm{R} = 1.000$ and near the rotor plane at $z/\mathrm{R} = 0.050$ (in the filtered and non-filtered cases) are compared with the altered spectrum modeled by the RDT from upstream flow conditions.

obtained using the HWA frequency spectra as input on the whole frequency range where TIN dominates, proving the validity of the proposed approach.

As expected, the alteration undergone by turbulence as it approaches the rotor due to the streamtube contraction leads to different results in the prediction. The implementation of Amiet's model with the velocity spectrum sampled far upstream yields a slight overprediction in the low-frequency range. In contrast, the velocity spectrum sampled near the rotor plane leads to a more accurate prediction in this frequency range. Such an effect plays a significant role in cases for which the variation of section of the streamtube is particularly pronounced, as in hovering conditions or high-speed rotation regimes. Figure 11 also shows Amiet's model implemented with the distorted spectrum obtained through RDT, which closely matches the prediction obtained using the downstream HWA spectra as input. This analysis demonstrates how the modified Amiet's model can be used to evaluate the impact of the inflow conditions on the acoustic spectra through direct HWA measurements.

IV. CONCLUSIONS

A modification to Amiet's model for TIN prediction in rotors is proposed to directly use probe measurements of the inflow conditions as inputs. This formulation enables the model to be applied to complex configurations with limited turbulence modeling and measurement availability. It is achieved by transforming the original 3D turbulence spectrum used as input into a 1D one. This conversion is made possible by using an inverse strip theory approach and introducing two auxiliary functions, i.e., the axial and spanwise correlation length. The former describes the radial correlation of the velocity fluctuations perpendicular to the rotor plane, while the latter accounts for the blade-to-blade correlation.

The proposed methodology is validated using experimental measurements of a two-bladed propeller interacting with grid-generated turbulence at three different advance ratios. Good agreement is found between the experimental measurements and the modified Amiet's model at all the considered advance ratios. This result proves the validity of the present model for an axial-flight configuration, which is

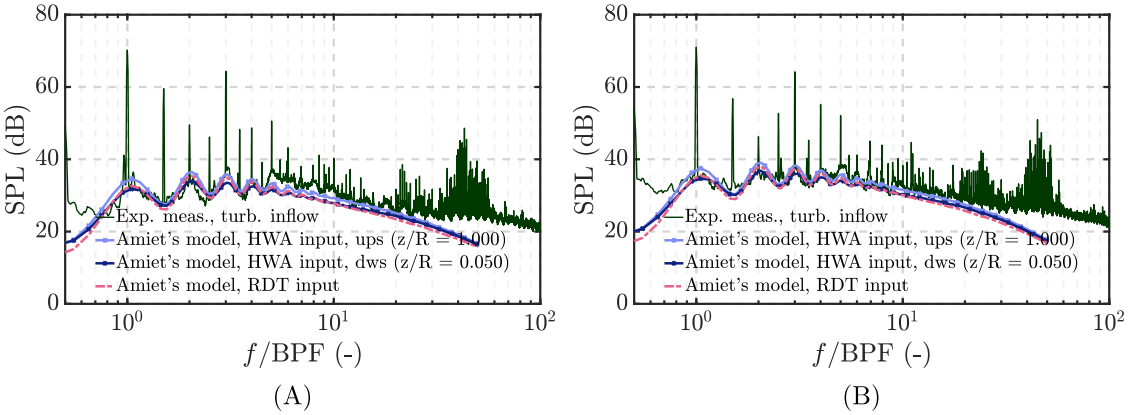

FIG. 11. Sound pressure level predicted by Amiet's model applied using HWA spectra sampled far upstream ($z/\mathrm{R} = 1.000$) and near the rotor plane ($z/\mathrm{R} = 0.050$) compared to experimental measurements at $\Omega = 6000$ RPM for (A) $\theta = 60°$ (microphone 1), (B) $\theta = 130°$ (microphone 8). The comparison includes the prediction using the altered velocity spectrum from the RDT as input. The reference pressure used to calculate the SPL is 2×10^{-5} Pa.

characterized by less pronounced distortion due to streamtube contraction. Additional validation would still be necessary to assess the robustness of the methodology in conditions where such effects are more pronounced, such as during hovering flight.

While converting the 3D turbulence term into a 1D spectrum through the introduction of auxiliary functions may seem like an added complexity and a limiting simplification, it actually creates a flexible and robust framework for applying this modified low-fidelity prediction tool. Two key points should be highlighted in this regard. First, the velocity spectrum is the key quantity to accurately describe for noise prediction, as the spanwise coherence length directly influences noise levels, while the axial correlation length serves as a transformation function that accounts for haystacking effects. Second, this formulation is intended to be used within a strip theory framework. Under these conditions, the assumption of homogeneous and isotropic turbulence used to introduce the axial correlation length becomes more justifiable, given that the inflow conditions can reasonably be considered piecewise homogeneous and isotropic. Moreover, the robustness of the model beyond such hypotheses, i.e., under non-homogeneous and anisotropic flow conditions, is supported by the accurate results obtained using probe measurements taken near the rotor plane and the RDT spectrum as input, both of which represent altered turbulence conditions.

The result is, hence, a formulation that configures Amiet's model as a modular tool, where the various contributions affecting the turbulence interacting with the rotor and the resulting noise scattering are represented by decoupled terms. This enables the individual investigation and modeling of each physical mechanism and its relative impact on noise generation. While currently focused on improving the description and modeling of the input turbulence term, the proposed modification broadens the potential of the model for new applications. Upon adequate validation or adaptation, the inherent structure of the model makes it indeed well suited for complex configurations, such as propellers in vortex-ring state, rotors ingesting boundary layers, contra-rotating propeller cases, and strongly anisotropic inflow conditions, as limited inflow measurements are required for its application.

Furthermore, in its current state, the proposed framework lays the ground for combining different models available in the literature to describe the successive phases of turbulence alteration as it approaches the rotor. For instance, the deformation due to the streamtube contraction can be taken into account through the RDT into the velocity spectrum term, while the multiple chopping of the elongated turbulent eddies is modeled through the axial correlation length. In addition, future developments could focus on characterizing the interaction between the chopped elongated turbulent structures and the leading edge, which can now be incorporated through the conversion of turbulence input into a 1D spectrum. The potential to account for such a mechanism, particularly relevant for cases introducing significant flow disturbances, would make the proposed model especially well suited to capture the effects of blades with realistic shapes and complex rotor geometries.

ACKNOWLEDGEMENTS

The authors gratefully acknowledge the European Commission for financial support provided through the Horizon 2020 Marie Skłodowska-Curie Innovative Training Network project "zEPHYR" (Grant No. 860101). The authors also wish to thank Dr. Özgür Yalçın from Delft University of Technology for his significant contribution to the implementation of the model and Sara Montagner and Mario Alì from Politecnico of Turin for their support during the experimental campaign.

AUTHOR DECLARATIONS

Conflict of Interest

The authors have no conflicts to disclose.

DATA AVAILABILITY

The data that support the findings of this study are available from the corresponding author upon reasonable request.

Amiet, R. K. (**1975**). "Acoustic radiation from an airfoil in a turbulent stream," J. Sound Vib. **41**(4), 407–420.
Amiet, R. K. (**1976**). "Noise produced by turbulent flow into a propeller or helicopter rotor," in *3rd Aeroacoustics Conference, Aeroacoustics Conferences*, Palo Alto, CA (July 20–23, 1976) (American Institute of Aeronautics and Astronautics, Reston, VA).
Amiet, R. K. (**1989**). "Noise produced by turbulent flow into a rotor: Theory manual for noise calculation," NASA Contractor Report 181788 (United Technologies Research Center, East Hartford, CT).
Amiet, R. K., Simonich, J. C., and Schlinker, R. H. (**1990**). "Rotor noise due to atmospheric turbulence ingestion. II - Aeroacoustic results," J. Aircr. **27**(1), 15–22.
Batchelor, G. K., and Proudman, I. (**1954**). "The effect of rapid distortion of a fluid in turbulent motion," Q. J. Mech. Appl. Math. **7**(1), 83–103.
Boucher, M. A., Christian, A. W., Krishnamurthy, S., Tracy, T., Begault, D. R., Shepherd, K., and Rizzi, S. A. (**2024**). "Toward a psychoacoustic annoyance model for urban air mobility vehicle noise," available at https://ntrs.nasa.gov/citations/20240003202.
Brooks, T. F., and Burley, C. L. (**2004**). "Blade wake interaction noise for a main rotor," J. Am. Helicopter Soc. **49**(1), 11–27.
Casalino, D., Romani, G., Zhang, R., and Chen, H. (**2022**). "Lattice-Boltzmann calculations of rotor aeroacoustics in transitional boundary layer regime," Aerosp. Sci. Technol. **130**, 107953.
Christophe, J., Anthoine, J., and Moreau, S. (**2009**). "Amiet's theory in spanwise-varying flow conditions," AIAA J. **47**(3), 788–790.
dos Santos, F. L., Botero-Bolívar, L., Venner, C., and de Santana, L. (**2022**). "Modeling the turbulence spectrum dissipation range for leading-edge noise prediction," AIAA J. **60**, 3581–3592.
Glegg, S. A. L., and Devenport, W. J. (**2017**). *Aeroacoustics of Low Mach Number Flows* (Academic Press, London, UK).
Glegg, S. A. L., Devenport, W. J., and Alexander, W. N. (**2015**). "Broadband rotor noise predictions using a time domain approach," J. Sound Vib. **335**, 115–124.
Glegg, S. A. L., Kawashima, E., Lachowski, F., and Devenport, W. J. (**2013**). "Propeller noise: Inflow distortion in a non axisymmetric flow," in *19th AIAA/CEAS Aeroacoustics Conference*, Berlin, Germany (May 27-29, 2013) (American Institute of Aeronautics and Astronautics, Reston, VA).

Goldschmidt, J., Tingle, H., Ifgu, P. G., Miller, S. A., Ukeiley, L. S., Goldman, B., Droandi, G., and Lee, K. (**2022**). "Acoustics and forces from an isolated rotor system," in *AIAA SCITECH 2022 Forum*, San Diego, CA (January 3–7, 2022) (American Institute of Aeronautics and Astronautics, Reston, VA).

Goldstein, M. E. (**1978**). "Unsteady vortical and entropic distortions of potential flows round arbitrary obstacles," J. Fluid Mech. **89**(3), 433–468.

Grande, E., Ragni, D., Avallone, F., and Casalino, D. (**2022a**). "Laminar separation bubble noise on a propeller operating at low Reynolds numbers," AIAA J. **60**(9), 5324–5335.

Grande, E., Romani, G., Ragni, D., Avallone, F., and Casalino, D. (**2022b**). "Aeroacoustic investigation of a propeller operating at low Reynolds numbers," AIAA J. **60**(2), 860–871.

Greenwood, E., Brentner, K. S., Rau, R. F., II, and Ted Gan, Z. F. (**2022**). "Challenges and opportunities for low noise electric aircraft," Int. J. Aeroacoust. **21**(5–7), 315–381.

Hanson, D. B. (**1974**). "Spectrum of rotor noise caused by atmospheric turbulence," J. Acoust. Soc. Am. **55**(S1), S3–S4.

Homicz, G. F., and George, A. R. (**1974**). "Broadband and discrete frequency radiation from subsonic rotors," J. Sound Vib. **36**(2), 151–177.

Kücükcoskun, K. (**2012**). "Prediction of free and scattered acoustic fields of low-speed fans," Doctoral thesis, Ecole Centrale de Lyon, Lyon, France.

Majumdar, S. J., and Peake, N. (**1998**). "Noise generation by the interaction between ingested turbulence and a rotating fan," J. Fluid Mech. **359**, 181–216.

Merino-Martínez, R., Rubio Carpio, A., Lima Pereira, L. T., Van Herk, S., Avallone, F., Ragni, D., and Kotsonis, M. (**2020**). "Aeroacoustic design and characterization of the 3D-printed, open-jet, anechoic wind tunnel of Delft University of Technology," Appl. Acoust. **170**, 107504.

Paterson, R. W., and Amiet, R. K. (**1982**). "Noise of a model helicopter rotor due to ingestion of isotropic turbulence," J. Sound Vib. **85**(4), 551–577.

Piccolo, A., Zamponi, R., Avallone, F., and Ragni, D. (**2024**). "Turbulence distortion and leading-edge noise," Phys. Fluids. **36**, 125183.

Raposo, H., and Azarpeyvand, M. (**2024**). "Turbulence ingestion noise generation in rotating blades," J. Fluid Mech. **980**, A53.

Rizzi, S. A., Huff, D. L., Boyd, D. D., Jr., Bent, P., Henderson, B. S., Pascioni, K. A., Sargent, D. C., Josephson, D. L., Marsan, M., He, H. (b.), and Snider, R. (**2020**). "Urban air mobility noise: Current practice, gaps, and recommendations," available at https://ntrs.nasa.gov/citations/20205007433.

Santana, L. D., Christophe, J., Schram, C., and Desmet, W. (**2016**). "A rapid distortion theory modified turbulence spectra for semi-analytical airfoil noise prediction," J. Sound Vib. **383**, 349–363.

Sharland, I. J. (**1964**). "Sources of noise in axial flow fans," J. Sound Vib. **1**(3), 302–322.

Simonich, J. C., Amiet, R. K., Schlinker, R. H., and Greitzer, E. M. (**1986**). "Helicopter rotor noise due to ingestion of atmospheric turbulence," available at https://ntrs.nasa.gov/citations/19860015745.

Simonich, J. C., Amiet, R. K., Schlinker, R. H., and Greitzer, E. M. (**1990**). "Rotor noise due to atmospheric turbulence ingestion. I - Fluid mechanics," J. Aircr. **27**, 7–14.

Sinayoko, S., Kingan, M., and Agarwal, A. (**2013**). "Trailing-edge noise theory for rotating blades in uniform flow," Proc. R. Soc. A **469**, 20130065.

Thurman, C., Wang, L., and Padway, E. (**2025**). "Broadband noise prediction of two small hovering rotors using FUN3D-ANOPP2," in *AIAA SCITECH 2025 Forum*, Orlando, FL (American Institute of Aeronautics and Astronautics, Reston, VA).

von Kármán, T. (**1948**). "Progress in the statistical theory of turbulence," in *Proceedings of the National Academy of Sciences*, Vol. 34, pp. 530–539.

Wilson, D. K. (**1997**). "Three-dimensional correlation and spectral functions for turbulent velocities in homogeneous and surface-blocked boundary layers," Technical Report, Army Research Laboratory, Adelphi, MD.

Zamponi, R., Moreau, S., and Schram, C. (**2021**). "Rapid distortion theory of turbulent flow around a porous cylinder," J. Fluid Mech. **915**, A27.

Zamponi, R., Satcunanathan, S., Moreau, S., Ragni, D., Meinke, M., Schröder, W., and Schram, C. (**2020**). "On the role of turbulence distortion on leading-edge noise reduction by means of porosity," J. Sound Vib. **485**, 115561.

Zawodny, N. S., Boyd, D. D., and Burley, C. L. (**2016**). "Acoustic characterization and prediction of representative, small-scale rotary-wing unmanned aircraft system components," in *American Helicopter Society (AHS) Annual Forum*, West Palm Beach, FL, available at https://ntrs.nasa.gov/citations/20160009054.